Geophysical Research Letters

RESEARCH LETTER
10.1029/2019GL082126

Interplanetary Shock Parameters Near Jupiter's Orbit

E. Echer[1]

[1]Instituto Nacional de Pesquisas Espaciais (INPE), São José dos Campos, Brazil

Abstract Fast interplanetary shocks occurrence, their parameters, and drivers near Jupiter's orbit are determined in this paper. It was found that 70% of the fast shocks are forward (FS) and 30% are reverse (RS). Interplanetary coronal mass ejection-driven FS occur more frequently in all solar cycle phases except in the declining phase, when corotating interaction region-driven shocks predominate. Most of the shocks were quasi-perpendicularly (65° to 70°) propagating relative to the ambient interplanetary magnetic field. The average shock magnetosonic Mach number is slightly higher for FS (2.6) than for RS (2.4), which in turn are stronger than shocks near 1 and 10 AU reported in previous works. This occurs because of the full development of corotating interaction region shocks and higher occurrence of strong interplanetary coronal mass ejections near 5 AU and that the magnetosonic speed at 5 AU has only 60% of its value at 1 AU.

Plan Language Summary Interplanetary shock waves are sudden variations in solar wind plasma and magnetic field parameters. They propagate in the interplanetary space and have important effects on planetary magnetospheres. For instance, shocks cause expansions and compressions of Jupiter's magnetosphere and trigger its auroral emissions. In this work plasma and magnetic field data from several spacecraft that crossed interplanetary space near Jupiter's orbit space are analyzed. A list of interplanetary shocks is compiled, and their parameters and drivers are determined. It was found that shocks at 5 AU have preferentially a quasi-perpendicular propagation to the magnetic field direction and are on average stronger than shocks observed near Earth's orbit.

Key Points:
- Interplanetary shock occurrence, parameters, and drivers near Jupiter's orbit are determined
- There are about 70% fast forward and 30% reverse shocks; about 90% of RS are CIR driven, while 45% of FS are CIR driven and 55% are ICME driven
- Shocks at 5 AU are mostly quasi-perpendicularly propagating and stronger on average than shocks at 1 AU

Supporting Information:
- Supporting Information S1

Correspondence to:
E. Echer,
ezequiel.echer@inpe.br;
ezequiel.echer@gmail.com

Citation:
Echer, E. (2019). Interplanetary shock parameters near Jupiter's orbit. *Geophysical Research Letters*, *46*. https://doi.org/10.1029/2019GL082126

Received 28 JAN 2019
Accepted 10 MAY 2019
Accepted article online 16 MAY 2019

1. Introduction

In the interplanetary space, a fast shock will form when the speed of its driver relative to the ambient solar wind is higher than the fast magnetosonic wave speed (V_{ms}) of the medium (Colburn and Sonnett, 1966; Kennell et al., 1985; Tsurutani et al., 2011). The main interplanetary shock drivers are interplanetary coronal mass ejections (ICMEs) or corotating interaction regions (CIRs), formed when fast streams overtake slower solar wind (Burlaga, 1995; Tsurutani et al., 2011).

It is known that the structure of the solar wind changes between 1 and 5 AU (the orbit of Jupiter) and beyond, including the development of CIR shocks from ~2–3 AU onward (Burlaga, 1995; Echer, 2019; Gosling et al., 1976; Luhmman, 1995; Neugebauer, 2013; Richardson et al., 2008; Smith & Wolfe, 1976; Smith, 1985). Further, the interplanetary shock and ICME characteristics also change with radial distance (Gazis & Lazarus, 1983; Richardson, 2011; Richardson, 2014; Whang, 1991; Whang & Burlaga, 1999). Interplanetary shocks, due to their important effects on space weather (Echer et al., 2004, 2005, 2008; Huttunen & Koskinen, 2004; Kilpua et al., 2017; Tsurutani et al., 1988), have been extensively studied near 1 AU (Bavassano-Cattaneo et al., 1986; Echer et al., 2003, 2004, 2011; Kilpua et al., 2015; Tsurutani & Lin, 1985). On the other hand, there have been fewer studies of shocks near 5 AU (Balogh et al., 1995; Echer, Zarka, et al., 2010; Echer, Tsurutani, et al., 2010; González-Esparza et al., 1996, 1998).

Such shocks are of interest because, although Jupiter's magnetosphere is largely controlled by its fast rotation and internal plasma sources, it also responds partially to solar wind variations (Bagenal, 2007; Khurana et al., 2004; Krupp et al., 2004). For example, solar wind dynamic pressure (P_{sw}) variations cause changes in the bow shock/magnetopause position (Ebert et al., 2014; Joy et al., 2002; McComas et al., 2014), and interplanetary shock arrival can trigger UV and radio auroral activities (Clarke et al., 2009; Echer, Zarka, et al., 2010; Hess et al., 2012, 2014, and references therein).

Therefore, it is the aim of the present paper to compile a list of interplanetary shocks near Jupiter's orbit (5 AU), and to study their parameters and possible drivers. In situ high-resolution plasma and interplanetary magnetic field (IMF) data that crossed interplanetary space near Jupiter's orbit from 1973 to 2004 are used

Table 1
Spacecraft Data Intervals Selected Near Jupiter's Orbit

S/C	Selected interval	Solar cycle phase	Jupiter closest approach	Interval excluded	N. shocks
Pioneer-10	275/1973-210/1974	Minimum	338/1973 (4 December 1973)	330-356/1973	27
Voyager-1	353/1978-149/1979	Maximum	064/1979 (5 March 1979)	059-081/1979	13
Voyager-2	067/1979-261/1979	Maximum	190/1979 (9 July 1979)	183-215/1979	10
Ulysses (U_A)	330/1991-117/1992	Maximum	039/1992 (8 February 1992)	033-048/1992	15
Ulysses (U_B)	154/1997-187/1998	Rising	X	X	30
Ulysses (U_C)	225/2003-255/2004	Declining	X	X	53

in this work. The results are compared with previous works analyzing interplanetary shocks at other heliocentric distances.

2. Methodology and Data Analysis

2.1. Data Interval Selection

Solar wind data near Jupiter's orbit were selected from heliospheric distance range from 4.8 to 5.6 AU, and in the heliolatitude range of ±10° in relation to the ecliptic plane. Available solar wind data from spacecraft in these coordinates were downloaded through the Space Physics Data Facility at the Goddard Space Flight Center/NASA (https://cohoweb.gsfc.nasa.gov/coho/). Data were selected only from spacecraft that have simultaneously high resolution (~1 to 5 min) plasma and magnetic field data.

Table 1 shows the selected spacecraft intervals according to the above mentioned heliolatitude and distance criteria. In this table, columns are selected intervals in year and day of year, the time of Jupiter closest approach, the solar cycle phase of each interval, the periods excluded because the spacecraft were in the Jupiter's magnetosphere, and the number of interplanetary shocks identified for each interval. Note that Pioneer-10, Voyager-1, and Voyager-2 made Jupiter flybys, while Ulysses orbited the Sun in a high-inclination orbit after an initial flyby (U_A interval), and then crossed the ecliptic plane near ~5 AU (but far from Jupiter) on two other periods (U_B and U_C intervals).

2.2. Shock Analysis Methods

In this paper, the methodology of shock analysis follows that presented in previous works (Echer et al., 2003; Echer, Zarka, et al., 2010; Echer, Tsurutani, et al., 2010, 2011; Echer, 2019). First, a list of shocks is compiled. This was performed by looking at high-resolution IMF and plasma data. Sudden variations in plasma and field parameters are marked by hand and the event is classified as a discontinuity. When there is a positive jump (in time) in all parameters (solar wind speed, V_{sw}, solar wind proton density N_p, solar wind proton temperature T_p, and IMF magnitude B_o) in the spacecraft frame, the discontinuity is classified as a potential fast forward shock (FS). On the other hand, when there is a positive jump in V_{sw}, but negative jumps in T_p, N_p, and B_o, it is classified as a potential fast reverse shock (RS).

The shock ramp is delimited as an interval of about 5 to 10 min, when there is a sudden discontinuity in plasma and field data. These parameters are averaged in upstream and downstream intervals of about 10 min around the shock ramp. In these intervals, careful analysis was made to eliminate periods with large discontinuities or fluctuations that could contaminate shock normal analysis (Echer, Zarka, et al., 2010; Echer, Tsurutani, et al., 2010, 2011; Tsurutani & Lin, 1985; Tsurutani et al., 2011).

After determining the averaged upstream and downstream plasma and field parameters, the shock normal is calculated using the mixed-mode technique (Abraham-Shrauner, 1972; Abraham-Shrauner & Yun, 1976; Tsurutani et al., 2011; Tsurutani & Lin, 1985). This method employs both upstream (1) and downstream (2) plasma and magnetic field vector data, and it has been found to give better results than the magnetic coplanarity technique (Tsurutani & Lin, 1985).

After determining the shock normal, the angle θ_{Bn} between it and the upstream IMF vector is determined. Then shocks are classified as quasi-parallel ($\theta_{Bn} \leq 45°$) or quasi-perpendicular $\theta_{Bn} > 45°$ propagating relative to the upstream IMF vector. After, the magnetosonic Mach number $M_{ms} = V_s/V_{ms}$ is computed, where V_s is the shock speed along the shock normal relative to the upstream solar wind and V_{ms} is the magnetosonic speed, computed from the Alfven and sound speed and taking into account the shock normal angle θ_{Bn}

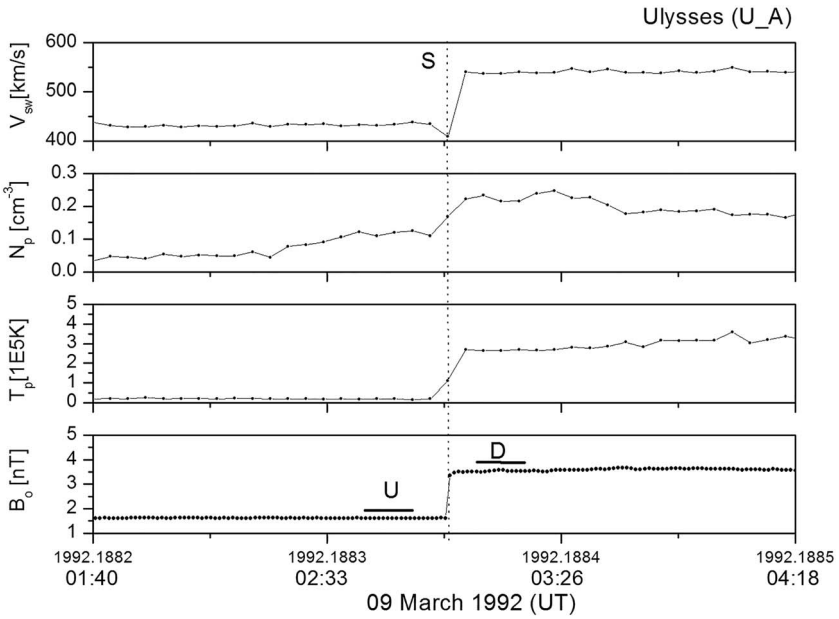

Figure 1. Fast forward interplanetary shock observed during Ulysses first selected interval. The shock ramp (S), and the upstream (U) and downstream (D) intervals are marked with dotted lines and with horizontal bars. This shock occurs at ~03:00 UT on 9 March 1992.

(for more details see Echer, Zarka, et al., 2010; Echer, Tsurutani, & Guarnieri, 2010, 2011; Tsurutani & Lin, 1985; Tsurutani et al., 2011). If $M_{ms} > 1$, the discontinuity is classified as a shock and is kept in the final shock list. Further, in order to characterize the shock strength, besides the M_{ms}, plasma density and IMF strength downstream to upstream ratios, $r_N = N_2/N_1$ and $r_B = B_2/B_1$, are also computed.

To identify possible shock drivers, solar wind high-resolution data plots are inspected by eye and the drivers classified as ICME or CIR according to known criteria (Burlaga, 1995; Echer et al., 2008; Kilpua et al., 2017): for ICMEs, some of the criteria are high values of magnetic field, low plasma T_p, and large-scale rotation of the field (for magnetic clouds, see Burlaga's book chapter 6); for CIRs, the occurrence of slow and fast solar wind V_{sw} intervals is separated by a region of compressed N_p and B_o (Smith, 1985). Further, the list of ICMEs observed by Ulysses from Richardson (2014) work has been used to help to identify the shock drivers, especially for ICMEs that are not magnetic clouds. Shocks are then classified in FS ICME or CIR driven (ICME-FS and CIR-FS) and RS ICME or CIR driven (ICME-RS and CIR-RS).

Figure 1 shows an example of interplanetary shock identification. Panels are V_{sw}, N_p, T_p, and B_o from Ulysses first interval (U_A). The magnetic field data have a 1-min resolution, while the plasma data have an ~5-min resolution. The interplanetary shock is identified with a vertical dotted line in all panels and by the "*S*" letter. The upstream (1) and downstream (2) intervals selected to perform the shock analysis are marked with horizontal bars and "*U*" and "*D*" letters, respectively. It can be seen that there is a strong jump in all parameters. This shock occurred at ~03:00 UT on day 069/1992. It was a quasi-perpendicular ($\theta_{Bn} = 65°$) and relatively strong ($r_N = 1.7$; $r_B = 2.2$; $M_{ms} = 2.7$) shock. This shock was driven by an ICME (ICME-FS).

A list of all interplanetary shocks, containing its time of occurrence, observing spacecraft, the type of shock (FS or RS), and calculated parameters: shock normal angle θ_{Bn}, magnetosonic Mach number M_{ms} and compression ratios (plasma r_N and field strength r_B), is available on request to the author or as supporting information. This list of shocks could be used in joint studies with other databases such as the http://ipshocks.fi list (Kilpua et al., 2015).

3. Results

During the period of the analysis, 148 shocks have been identified: 46 RS (31%) and 102 FS (69%). In another study of shocks at the ecliptic plane, also at 5 AU, focused on the post maximum solar cycle phase (2003–

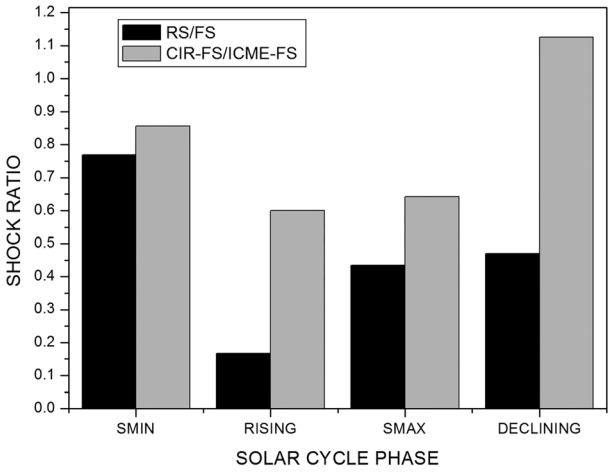

Figure 2. Distribution with solar cycle phase of the RS/FS (total) ratio and the CIR-FS/ICME-FS ratio. RS = reverse shock; FS = forward shock; CIR = corotating interaction region; ICME = interplanetary coronal mass ejection.

2004), Echer, Zarka, et al. (2010) have found for a limited interval that ~72% of shocks were FS and ~28% were RS, which is also similar to the results obtained in this paper. For comparison, at 1 AU, the proportion of FS and RS was 88% to 10% in solar maximum and 66% to 33% in solar minimum (Echer et al., 2003). Further, Kilpua et al. (2015), also at 1 AU, have observed that FS occurrence is higher than RS in all solar cycle phases except at solar minimum: 76% of all analyzed shocks over the whole 19-year period were FS. At 10 AU (Echer, 2019), it was noted from Voyager-1 and Voyager-2 (near solar maximum) data that there was an occurrence of 75% of FS and 25% RS.

Based on the identification criteria for CIRs and ICMEs (outlined in section 2), the solar wind plots were analyzed to identify the possible driver of each interplanetary shock. A small number of shocks (14 of 148, or ~10%) could not have their driver unambiguously identified, due to data gaps or complex interplanetary structures.

From the remaining shocks, the number of shocks for each driver was ICME-FS, 52; ICME-RS, 4; CIR-FS, 42, and CIR-RS, 36. It can be seen that at 5 AU the vast majority of RS are driven by CIRs (~90%) with only a few cases being ICME driven. These ICME associated RS could be driven by speed difference between fast and slow solar wind plasma (Gosling et al., 1988) or by overexpansion of an ICME (Gosling et al., 1994). On the other hand, FS have a more equal distribution between ICME (55%) and CIR drivers (45%). Comparing with shock analysis results at 1 AU, Kilpua et al. (2015) have also found that the overwhelmingly majority (~94%) of RS are driven by CIRs, while most (~72%) of FS were driven by ICMEs. The difference in the FS drivers between 1 and 5 AU may be accounted because CIR shocks fully develop after ~2–3 AU (Smith & Wolfe, 1976); thus, the number of CIR FS at 5 AU should be higher, as observed in this work.

Another subject of interest regarding shock drivers is to study its solar cycle variation. The solar cycle phases for each spacecraft are defined as shown in Table 1. Figure 2 shows the RS to FS ratio according to solar cycle phase as well as the proportion of CIR-FS to ICME-FS-driven shocks.

From Figure 2 it can be seen that FS are predominant over RS in all solar cycle phases. It can also be seen that the relative proportion of RS to FS is higher at solar minimum and in declining phases. ICME-FS occur more often than CIR-FS in all phases, with exception of the declining phase. The proportion of CIR-FS to ICME-FS is higher at solar minimum and declining phases. This is in agreement to the expected effect of higher number of CIRs around these solar cycle phases. Kilpua et al. (2015) at 1 AU also found that FS dominate over RS in all solar cycle phases except during solar minimum. Also, ICME-driven shocks dominate in all phases, except at solar minimum when CIRs are more important.

Figure 3 shows histograms for ICME-FS, CIR-FS, and CIR-RS for θ_{Bn} and M_{ms}. The average, standard deviation, and median of the distributions are shown. As the number of ICME-RS is too small, it is not possible to derive their distribution. Their results however show that ICME-RS are weaker on average ($M_{\mathrm{ms}} = 1.8$) than other shock driver classes: $M_{\mathrm{ms}} = 2.5$ for ICME-FS, $M_{\mathrm{ms}} = 2.7$ for CIR-FS, and $M_{\mathrm{ms}} = 2.4$ for CIR-RS. Further, ICME-RS are also less perpendicularly propagating ($\theta_{Bn} = 55°$) than other shocks ($\theta_{Bn} = 66°$ for ICME-FS, $\theta_{Bn} = 67°$ for CIR-FS, and $\theta_{Bn} = 66°$ for CIR-RS).

It can be seen in the histograms in Figure 3 that most of all shocks (>80%) show quasi-perpendicular propagation. Further, more than 70% for all types of shocks have $\theta_{Bn} > 60°$. CIR-RS show a larger number of quasi-parallel shocks (15% against ~10% for other cases). Shock normal angle ranges from 15° to 90° for FS and from 7° to 90° for RS. Therefore, it is noted that shocks at 5 AU show mainly a quasi-perpendicular propagation, with shock normal angle of about 66° (~70° in median) for all FS and RS. These results are similar to 1 AU results obtained by Bavassano-Cattaneo et al. (1986), Neugebauer (2013), and Kilpua et al. (2015). In all those studies it was observed that the shock normal angle distribution showed an increasing occurrence rate of shocks for larger angles, that is, a higher number of quasi-perpendicular shocks than quasi-parallel shocks. At 10 AU, Echer (2019) also found a predominance of quasi-perpendicular shocks. This may

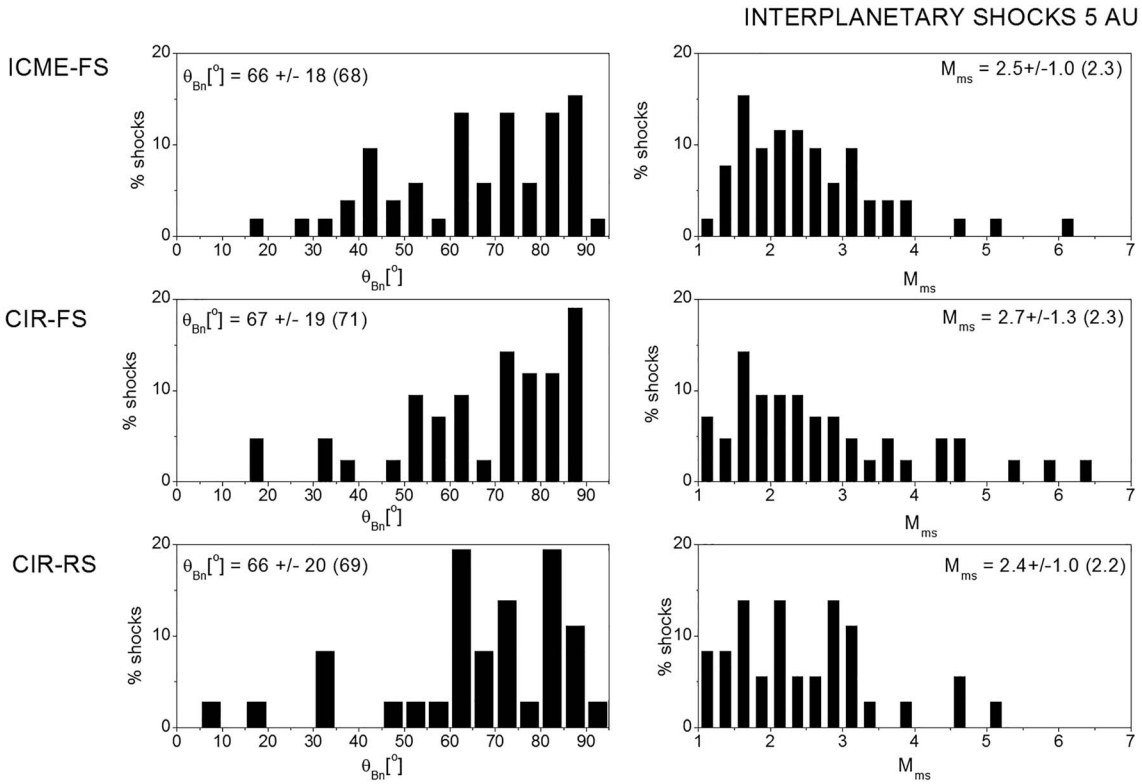

Figure 3. Histograms of shock normal angle θ_{Bn} (mixed mode, left column) and fast magnetosonic Mach Number M_{ms} (right column) for ICME-FS (top row), CIR-FS (middle row), and CIR-RS (bottom row) column. RS = reverse shock; FS = forward shock; CIR = corotating interaction region; ICME = interplanetary coronal mass ejection.

happen because IMF orientation is already on average ~45° to the radial distance at 1 AU and becomes more tangential at the outer heliosphere, making shock normal more likely to be quasi-perpendicular to the ambient IMF direction. Further, it should be mentioned that is also possible there is a small effect due to an identification bias, since perpendicular shocks have more clear jumps and are easier to spot than quasi-parallel ones (see Kilpua et al., 2015).

From Figure 3, it is seen that histograms for M_{ms} have a skewed to the right distribution, with few shocks at extreme values. It also can be noted that M_{ms} is slightly higher for ICME-FS (2.5) and CIR-FS (2.7) than for CIR-RS (2.4), similarly to what was noted in Echer, Zarka, et al. (2010) who have found for a limited interval that FS had average $M_{\mathrm{ms}} = 2.6$, and RS had $M_{\mathrm{ms}} = 2.4$. In fact, the M_{ms} distribution from Figure 3 shows that most shocks have values around $M_{\mathrm{ms}} = 1.5$–3.0 (71% of ICME-FS, 62% of CIR-FS, and 67% of CIR-RS).

Regarding shock compression ratio, it has been observed that they are similar for all FS (ICME-FS: $r_B = 2.3$ and CIR-FS, $r_B = 2.3$; ICME-FS: $r_N = 2.6$ and CIR-FS, $r_N = 2.5$; and for CIR-RS, $r_B = 2.2$ and $r_N = 2.7$). Their histograms (not show due to space limitation) also presented a skewed to the right distribution similar to the M_{ms} distributions.

In order to compare shocks strength at different heliocentric distances, results at 1, 5, and 10 AU from different works (see Figure 4 caption) were averaged and shown in Figure 4. In the top panel are plotted the average M_{ms} for FS and RS, and in the bottom panel, the shock compression ratios r_n and r_B.

It can be seen that on average FS have higher M_{ms} than RS for all distances. Further, M_{ms} increases from 1 to 5 AU and then declines to 10 AU. The same trend is noted when computing the plasma and magnetic field compression ratio (bottom panel). Thus, these results show that, on average, shock strength increases from 1 to 5 AU and then decreases from 5 to 10 AU. Discussion about the possible causes of this behavior is presented in section 4.

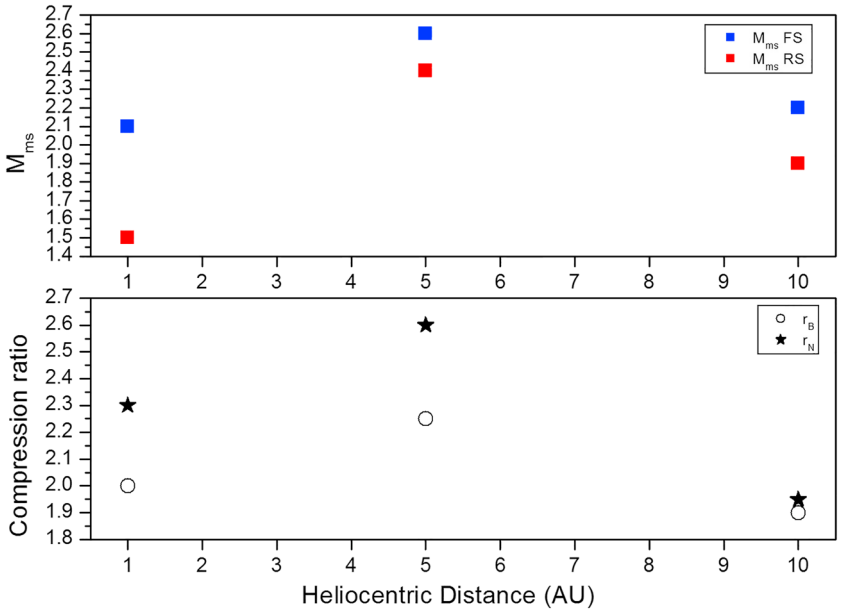

Figure 4. Shock strength versus heliocentric distance. (top) M_{ms} from Bavassano-Cattaneo et al. (1986) and Kilpua et al. (2015) for 1 AU, from this work for 5 AU and from Echer (2019) for 10 AU. (bottom) r_n and r_B at 1 AU (Echer et al., 2003), 5 AU (this work), and 10 AU (Echer, 2019). Note that errors are not given as these values are taken from different works and different databases.

Finally, correlations were calculated between several shock parameters (not shown due to space limitations). It was found that the correlation between shock strength parameters and shock normal angles is not significant, which implies that there is no clear relation between the shock being quasi-parallel or quasi-perpendicular and its strength in this data set. Higher and significant correlations are found between M_{ms} and r_B (0.64 for ICME-FS, 0.81 for CIR-FS). The correlations between shock r_n and r_B are $r = 0.55$ for ICME-FS, 0.55 for CIR-FS, and 0.73 for CIR-RS. This is expected since both plasma and field are compressed in shocks.

4. Summary and Conclusions

A study of interplanetary shock parameters near Jupiter's orbit has been conducted in this work. It was noted that there is a larger proportion of FS (70%) than RS (30%). Shock strength is slightly higher for FS (2.5-2.7) than for RS (2.4) but is higher than average shock strength at 1 or at 10 AU; most of shocks have quasi-perpendicular propagation angles (65–70°). Almost all (90%) RS are CIR driven, while 45% of FS are CIR driven and 55% are driven by ICMEs. ICME-driven FS have higher occurrence in all phases except in the declining phase. CIR FS- and RS-driven shocks occur preferentially around solar minima and declining phases. Shock parameters show significant correlation only between compression ratios, and between Mach number and magnetic field compression ratio.

Shock strength increasing from 1 to 5 AU and then leveling off afterwards has been previously observed (Gazis & Lazarus, 1983; Luhmman, 1995; González-Esparza et al., 1996; Hoang et al., 1995; Neugebauer, 2013). The reasons that the average shock strength is higher at 5 AU could be the decrease of V_{ms} with heliocentric distance from 1 to 5 AU and then leveling off from 5 to 10 AU (Echer, 2019), the full formation of CIR shocks after ~2-3 AU (Smith, 1985; Smith & Wolfe, 1976) and the fact that faster ICMEs have higher probability to propagate to larger distances (e.g., Neugebauer, 2013). Also, after 5 AU, it is noted that shock merging occurs more often and then shock strength can be reduced, as well as their occurrence rate (Burlaga, 1995; Echer, 2019; Neugebauer, 2013).

These results are of interest for researchers working on interplanetary dynamics at different heliocentric distances and on solar wind-Jupiter's magnetosphere coupling. They could be used to validate solar wind propagation models, for instance, mSWiM (Zieger & Hansen, 2008), comparing the predicted shock arrival time

and strength with real data, and to study interplanetary shocks in other regions of the heliosphere. Further, the results obtained in this paper are very important in the study of long-term (several solar cycles) solar wind Jupiter's magnetosphere coupling. This type of study could be conducted for example correlating the shock occurrence, type (RS or FS) and parameters determined in this work, with radio and UV observations of Jupiter's auroral activity, such as the Nançay radio data base (Marques et al., 2017), Hubble space telescope UV observations (Clarke et al., 2009), as well as radio and UV observations from several spacecraft (Voyager-1, Voyager-2, Galileo, Ulysses, Cassini, WIND, Stereo-A, and Stereo-B). Finally, these results may be useful to compare with recent interplanetary and auroral data collected with Juno spacecraft.

Acknowledgments
E. E. wishes to thank the CNPq and FAPESP agencies for financial support (contracts PQ-302583/2015-7 and 2018/21657-1, respectively) and to the Space Physics Data Facility at the Goddard Space Flight Center for the COHOWeb interplanetary plasma and magnetic field data.

References

Abraham-Shrauner, B. (1972). Determination of magnetohydrodynamic shock normals. *Journal of Geophysical Research*, *77*(4), 736–739. https://doi.org/10.1029/JA077i004p00736

Abraham-Shrauner, B., & Yun, S. H. (1976). Interplanetary shocks seen by Ames Plasma Probe on Pionneer 6 and 7. *Journal of Geophysical Research*, 2097–2102.

Bagenal, F. (2007). The magnetosphere of Jupiter: Coupling the equator to the poles. *Journal of Atmospheric and Solar - Terrestrial Physics*, *69*(3), 387–402. https://doi.org/10.1016/j.jastp.2006.08.012

Balogh, A., Gonzalez-Esparza, J. A., Forsyth, R. J., Burton, M. E., Goldstein, B. E., Smith, E. J., & Bame, S. J. (1995). Interplanetary shock waves: Ulysses observations in and out of the ecliptic plane. *Space Science Reviews*, *72*(1-2), 171–180. https://doi.org/10.1007/BF00768774

Bavassano-Cattaneo, M. B., Tsurutani, B. T., Smith, E. J., & Lin, R. P. (1986). Subcritical and supercritical interplanetary shocks; Magnetic field and energetic particle observations. *Journal of Geophysical Research*, *91*(A11), 11,929–11,935. https://doi.org/10.1029/JA091iA11p11929

Burlaga, L. F. (1995). *Interplanetary magnetohydrodynamics*, (p. 272). New York: Oxford University Press.

Clarke, J. T., Nichols, J., Gérard, J.-c., Grodent, D., Hansen, K. C., Kurth, W., et al. (2009). Response of Jupiter's and Saturn's auroral activity to the solar wind. *Journal of Geophysical Research*, *114*, A05210. https://doi.org/10.1029/2008JA01369

Colburn, D. S., & Sonnet, C. P. (1966). Discontinuity in the solar wind. *Space Science Reviews*, *5*, 439.

Ebert, R. W., Bagenal, F., McComas, D. J., & Fowler, C. M. (2014). A survey of solar wind conditions at 5 AU: a tool for interpreting solar wind-magnetosphere interactions at Jupiter. *Froniers in Astronomy and Space Sciences*, *1*(4), 1–13. https://doi.org/10.3389/fspas.2014.00004

Echer, E. (2019). Solar wind and interplanetary shock parameters near Saturn's orbit. *Planetary and Space Science*, *165*, 210–220. https://doi.org/10.1016/j.pss.2018.10.006

Echer, E., Alves, M. V., & Gonzalez, W. D. (2004). Geoeffectiveness of interplanetary shocks during solar minimum (1995-1996) and solar maximum (2000). *Solar Physics*, *221*(2), 361–380. https://doi.org/10.1023/B:SOLA.0000035045.65224.f3

Echer, E., Gonzalez, W. D., Guarnieri, F. L., Dal Lago, A., & Vieira, L. E. A. (2005). Introduction to space weather. *Advances in Space Research*, *35*(5), 855–865. https://doi.org/10.1016/j.asr.2005.02.098

Echer, E., Gonzalez, W. D., Tsurutani, B. T., & Gonzalez, A. L. C. (2008). Interplanetary conditions causing intense geomagnetic storms (Dst <−100 nT) during Solar Cycle 23 (1996-2006). *Journal of Geophysical Research*, *113*, A05221. https://doi.org/10.1029/2007JA012744

Echer, E., Gonzalez, W. D., Vieira, L. E. A., Dal Lago, A., Guarnieri, F. L., Prestes, A., et al. (2003). Interplanetary shock parameters during solar activity maximum (2000) and minimum (1995-1996). *Brazilian Journal of Physics*, *33*(1), 115–122. https://doi.org/10.1590/S0103-97332003000100010

Echer, E., Tsurutani, B. T., & Guarnieri, F. L. (2010). 2010b, Forward and reverse CIR shocks at 4-5 AU, Ulysses. *Advances in Space Research*, *45*(6), 798–803. https://doi.org/10.1016/j.asr.2009.11.011

Echer, E., Tsurutani, B. T., Guarnieri, F. L., & Kozyra, J. U. (2011). Interplanetary fast forward shocks and their geomagnetic effects: CAWSES events. *Journal of Atmospheric and Solar - Terrestrial Physics*, *73*(11-12), 1330–1338. https://doi.org/10.1016/j.jastp.2010.09.020

Echer, E., Zarka, P., Gonzalez, W. D., Morioka, A., & Denis, L. (2010). 2010a, Solar wind effects on Jupiter non-Io DAM emissions during Ulysses distant encounter (2003–2004). *Astronomy & Astrophysics*, *519*, A84. https://doi.org/10.1051/0004-6361/200913305

Gazis, P. R., & Lazarus, A. J. (1983). In M. Neugebauer (Ed.), *The radial evolution of the solar wind, 1-10 AU, Solar wind 5*, *NASA Conf. Publ*, (Vol. 2280, p. 505). Washington DC: NASA.

González-Esparza, J. A., Balogh, A., Forsyth, R. J., Neugebauer, M., Smith, E. J., & Phillips, J. L. (1996). Interplanetary shock waves and large-scale structures: Ulysses' observations in and out of the ecliptic plane. *Journal of Geophysical Research*, *101*(A8), 17,057–17,071. https://doi.org/10.1029/96JA00685

González-Esparza, J. A., Neugebauer, M., Smith, E. J., & Phillips, J. L. (1998). Radial evolution of ejecta characteristics and transient shocks: Ulysses in-ecliptic observations. *Journal of Geophysical Research*, *103*(A3), 4767–4773. https://doi.org/10.1029/97JA03271

Gosling, J. T., Bame, S. J., Mc Comas, D. J., Phillips, J. L., Scime, E. E., Pizzo, V. J., et al. (1994). A forward-reverse shock pair in the solar wind driven by over-expansion of a coronal mass ejection: Ulysses observations. *Geophysical Research Letters*, *21*(3), 237–240.

Gosling, J. T., Bame, S. J., Smith, E. J., & Burton, M. E. (1988). Forward-reverse shock pairs associated with transient disturbances in the solar wind at 1 AU. *Journal of Geophysical Research*, *93*(A8), 8741.

Gosling, J. T., Hundhausen, A. J., & Bame, S. J. (1976). Solar wind stream evolution at large heliocentric distances: experimental demonstration and test of a model. *Journal of Geophysical Research*, *81*(13), 2111–2122. https://doi.org/10.1029/JA081i013p02111

Hess, S. L. G., Echer, E., & Zarka, P. (2012). Solar wind pressure effects on Jupiter decametric radio emissions independent of Io. *Planetary and Space Science*, *70*(1), 114–125. https://doi.org/10.1016/j.pss.2012.05.011

Hess, S. L. G., Echer, E., Zarka, P., Lamy, L., & Delamere, P. A. (2014). Multi-instrument study of the Jovian radio emissions triggered by solar wind shocks and inferred magnetospheric subcorotation rates. *Planetary and Space Science*, *99*, 136–148. https://doi.org/10.1016/j.pss.2014.05.015

Hoang, S., Lacombe, C., Mangeney, A., Pantellini, F., Balogh, A., Bame, S. J., et al. (1995). Interplanetary shocks observed by Ulysses in the ecliptic plane as a function of the heliocentric distance. *Advances in Space Research*, *15*(8/9), 373–374.

Huttunen, K. E. J., & Koskinen, H. E. J. (2004). Importance of post-shock streams and sheath regions as driver of intense magnetospheric storms and high latitude activity. *Annales de Geophysique*, *22*(5), 1729–1738. https://doi.org/10.5194/angeo-22-1729-2004

Joy, S. P., Kivelson, M. G., Walker, R. J., Khurana, K. K., Russell, C. T., & Ogino, T. (2002). Probabilistic models of the Jovian magnetopause and bow shock locations. *Journal of Geophysical Research*, *107*(A10), 1309. https://doi.org/10.1029/2001JA009146

Kennell, C. F., Edmiston, J. P., & Hada, T. (1985). A quarter century of collisionless shock research, in *AGU Monograph*, 34, *Collisionless shocks in the heliosphere*, Ed. By R. G. Stone and B. T. Tsurutani, p.1-36. Washington, DC: American Geophysical Union.

Khurana, K. K., Kivelson, M. G., Vasyliunas, V. M., Krupp, N., Woch, J., Lagg, A., et al. (2004). The configuration of Jupiter's Magnetosphere (Chap. 24, pp. 593–616). In F. Bagenal, T. Dowling & W. McKinnon (Eds.). *Jupiter, the planet, satellites and magnetospheres*, Cambridge, UK: Cambridge University Press.

Kilpua, E. K. J., Balogh, A., von Steiger, R., & Liu, Y. D. (2017). Geoeffective Properties of Solar Transients and Stream Interaction Regions. *Space Science Reviews*, *212*(3-4), 1271–1314. https://doi.org/10.1007/s11214-017-0411-3

Kilpua, E. K. J., Lumme, E., Andreeova, K., Isavnin, A., & Koskinen, H. E. J. (2015). Properties and drivers of fast interplanetary shocks near the orbit of the Earth (1995-2013). *Journal of Geophysical Research: Space Physics*, *120*, 4112–4125. https://doi.org/10.1002/2015JA021138

Krupp, N., Vasyliunas, V. M., Woch, J., Lagg, A., Khurana, K. K., Kivelson, M. G., et al. (2004). Dynamics of the Jovian Magnetosphere (Chap. 25, pp. 617–638). In F. Bagenal, T. Dowling & W. McKinnon (Eds.). *Jupiter, the planet, satellites and magnetospheres*, Cambridge: Cambridge University Press.

Luhmman, J. G. (1995). Sources of interplanetary shocks. *Advances in Space Research*, *15*(8-9), 355–364. https://doi.org/10.1016/0273-1177(94)00117-J

Marques, M. S., Zarka, P., Echer, E., Ryabov, V. B., Alves, M. V., Denis, L., & Coffre, A. (2017). Statistical study of 26yr of observations of decametric radio emissions from Jupiter. *Astronomy & Astrophysics*, *604*(A17), 1–18.

McComas, D. J., Bagenal, F., & Ebert, R. W. (2014). Bimodal size of Jupiter's magnetosphere. *Journal of Geophysical Research: Space Physics*, *119*, 1523–1529. https://doi.org/10.1002/2013JA019660

Neugebauer, M. (2013). Propagating shocks. *Space Science Reviews*, *176*(1-4), 125–132. https://doi.org/10.1007/s11214-010-9707-2

Richardson, I. G. (2014). Identification of interplanetary coronal mass ejections at Ulysses using multiple solar wind signatures. *Solar Physics*, *289*(10), 3843–3894. https://doi.org/10.1007/s11207-014-0540-8

Richardson, J. D. (2011). Shocks and sheaths in the heliosphere. *Journal of Atmospheric and Solar - Terrestrial Physics*, *73*(11-12), 1385–1389. https://doi.org/10.1016/j.jastp.2010.06.005

Richardson, J. D., Liu, Y., & Wang, C. (2008). Solar wind structure in the outer heliosphere. *Advances in Space Research*, *41*(2), 237–244. https://doi.org/10.1016/j.asr.2007.03.069

Smith, E. J. (1985). Interplanetary shock phenomena beyond 1 AU. In *Collisionless shock in the heliosphere*, *AGU Geophysical Monograph Series*, (Vol. 35, pp. 69–83). Washington, DC: American Geophysical Union.

Smith, E. J., & Wolfe, J. H. (1976). Observations of interaction regions and corotating shocks between one and five AU: Pioneers 10 and 11. *Geophysical Research Letters*, *3*(3), 137–140. https://doi.org/10.1029/GL003i003p00137

Tsurutani, B. T., Gonzalez, W. D., Tang, F., Akasofu, S. I., & Smith, E. J. (1988). Origin of interplanetary southward magnetic fields responsible for major magnetic storms near solar maximum (1978–1979). *Journal of Geophysical Research*, *93*(A8), 8519–8531. https://doi.org/10.1029/JA093iA08p08519

Tsurutani, B. T., Lakhina, G. S., Verkhoglyadova, O. P., Gonzalez, W. D., Echer, E., & Guarnieri, F. L. (2011). A review of interplanetary discontinuities and their geomagnetic effects. *Journal of Atmospheric and Solar - Terrestrial Physics*, *73*(1), 5–19. https://doi.org/10.1016/j.jastp.2010.04.001

Tsurutani, B. T., & Lin, R. P. (1985). Acceleration of > 45 keV Ions and > 2 keV Electrons by interplanetary shocks at 1 AU. *Journal of Geophysical Research*, *90*(A1), 1–11. https://doi.org/10.1029/JA090iA01p00001

Whang, Y. C. (1991). Shock interactions in the outer heliosphere. *Space Science Reviews*, *57*(3-4), 339–388. https://doi.org/10.1007/BF00216047

Whang, Y. C., & Burlaga, L. F. (1999). Shocks in the distant heliosphere. *Journal of Geophysical Research*, *104*(A4), 6721–6727. https://doi.org/10.1029/1999JA900016

Zieger, B., & Hansen, K. C. (2008). Statistical validation of a solar wind propagation model from 1 to 10 AU. *Journal of Geophysical Research*, *113*, A08107. https://doi.org/10.1029/2008JA013046